ADVANCED ENERGY MATERIALS

Supporting Information

for *Adv. Energy Mater.*, DOI: 10.1002/aenm.201501873

Transparent Conductive Oxide-Free Graphene-Based Perovskite Solar Cells with over 17% Efficiency

*Hyangki Sung, Namyoung Ahn, Min Seok Jang, Jong-Kwon Lee, Heetae Yoon, Nam-Gyu Park, and Mansoo Choi**

Supporting Information

Transparent conductive oxide-free graphene-based perovskite solar cells over 17% efficiency

*Hyangki Sung, Namyoung Ahn, Min Seok Jang, Jong-Kwon Lee,b Heetae Yoon, Nam-Gyu Park, and Mansoo Choi**

H. Sung, N. Ahn, Prof. M. Choi
Department of Mechanical and Aerospace Engineering, Seoul National University, Seoul 08826, Korea.
E-mail: mchoi@snu.ac.kr
Dr. M. S. Jang, Dr. J.-K. Lee, Prof. M. Choi
Global Frontier Center for Multiscale Energy Systems, Seoul National University, Seoul 08826, Korea.
Prof. N.-G. Park
School of Chemical Engineering and Department of Energy Science, Sungkyunkwan University, Suwon 16419, Korea

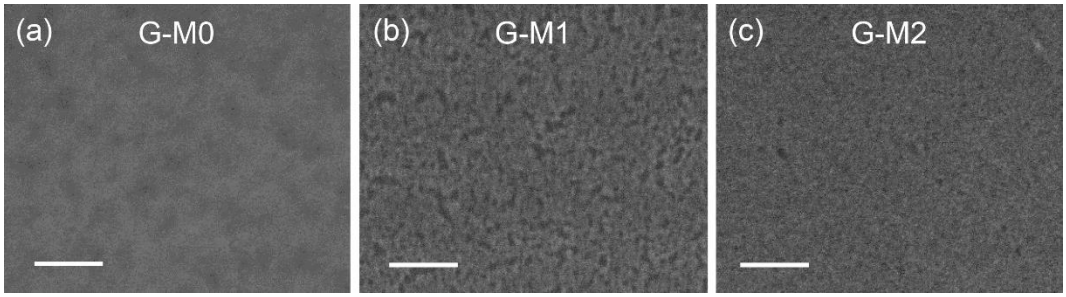

Figure S1. Plan-view SEM images of (a) as-prepared graphene, (b) graphene/1 nm MoO_3 and (c) graphene/2 nm MoO_3 (scale bar, 100 nm). The MoO_3 layers were deposited by thermal evaporation with deposition rate of 0.1 Å s^{-1}, followed by 150 °C annealing for 10 min.

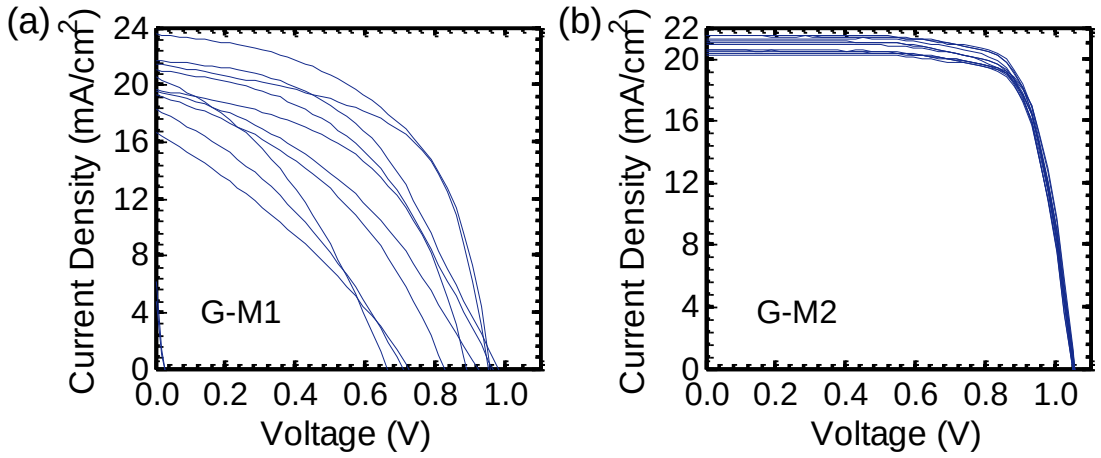

Figure S2. *J–V* curves of (a) G-M1 and (b) G-M2 devices under AM 1.5G illumination at 100 mW cm^{-2}. Non-consistent *J–V* characteristics appeared in G-M1 devices due to incomplete covering of 1 nm-thick MoO_3 layers over hydrophobic graphene surfaces, resulting in nonuniform formation of PEDOT:PSS and $MAPbI_3$ films.

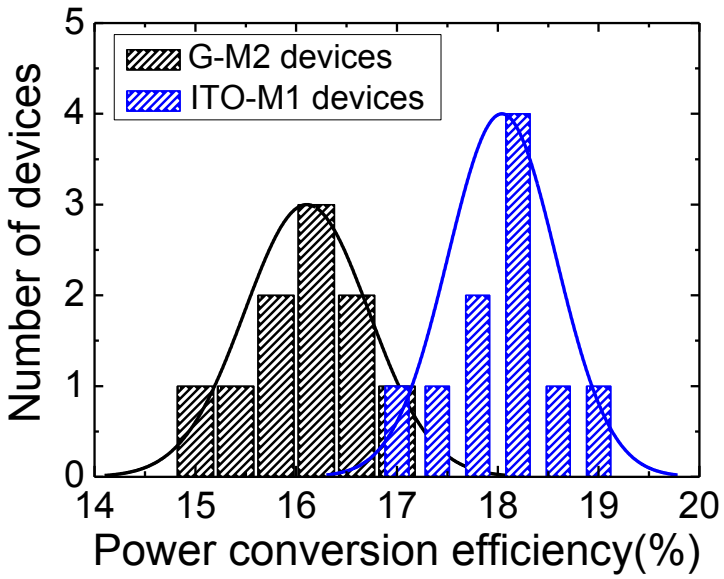

Figure S3. PCE Histogram of 10 devices for each electrode type, G-M2 and ITO-M1.

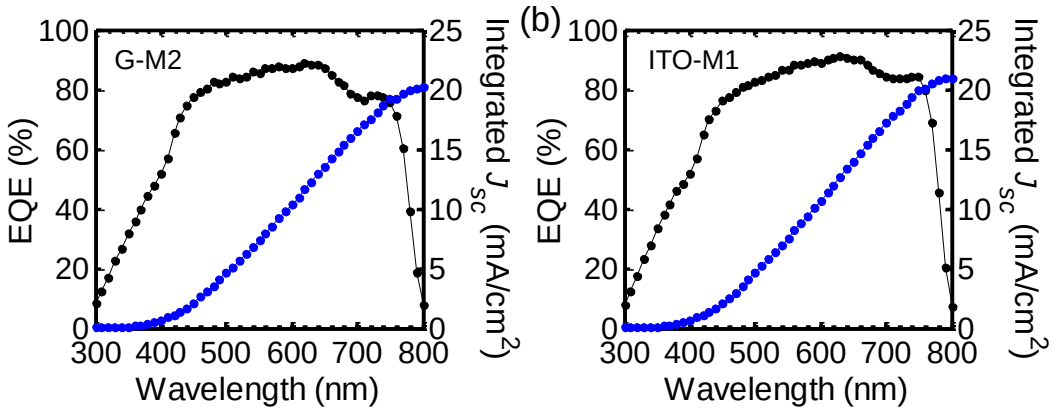

Figure S4. EQE spectra (black lines) and integrated J_{sc} (blue lines) of best-performing (a) G-M2 and (b) ITO-M1 devices. The integrated photocurrents were calculated as 20.2 and 21.0 mA cm^{-2}, respectively.

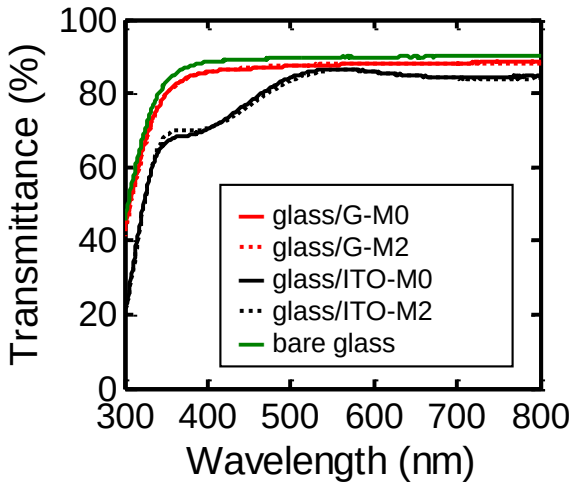

Figure S5. Transmittance of glass/graphene and glass/ITO with/without 2 nm-thick MoO_3 layers, and a bare glass substrate.

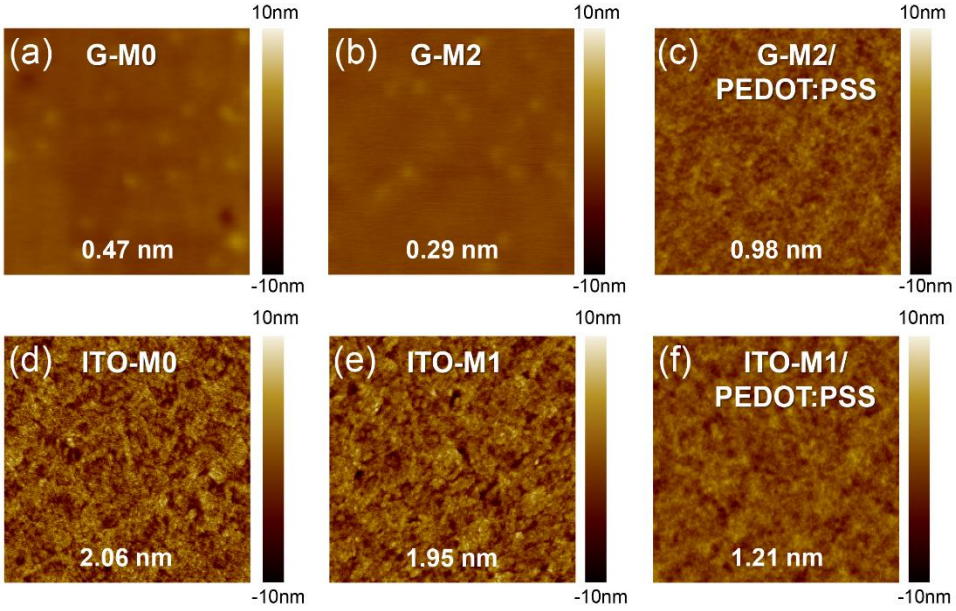

Figure S6. AFM topography images (3 μm × 3 μm) of (a) as-prepared graphene, (b) graphene/2 nm MoO_3, (c) graphene/2 nm MoO_3 after spin-coating of PEDOT:PSS, (d) as-prepared ITO, (e) ITO/1 nm MoO_3, (f) ITO/1 nm MoO_3 after spin-coating of PEDOT:PSS. The calculated surface rms roughness values were presented in each figure.

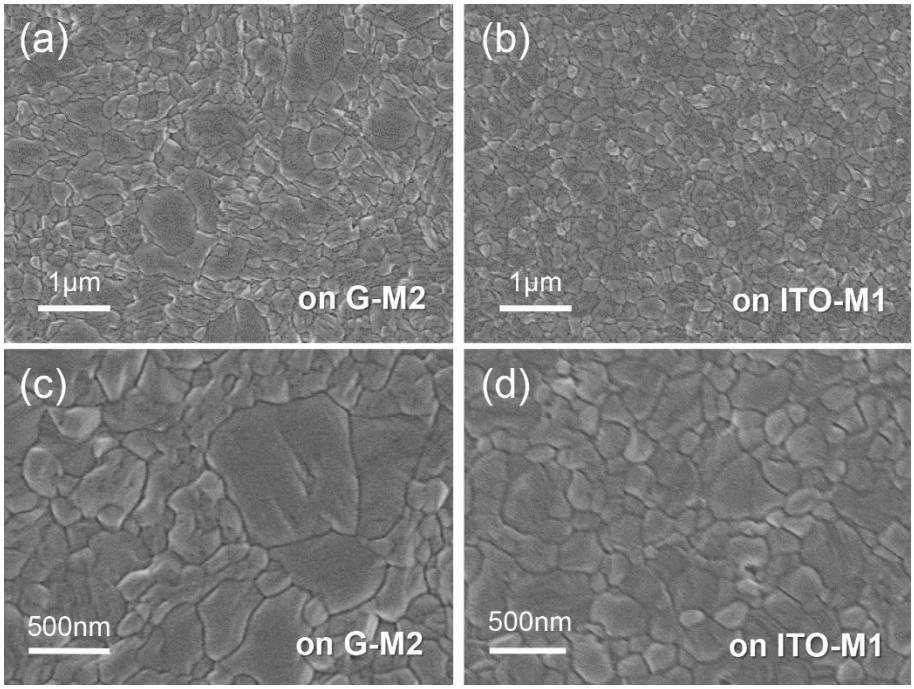

Figure S7. Plan-view SEM images of the $MAPbI_3$ perovskite films fabricated on (a) G-M2/PEDOT:PSS and (b) ITO-M1/PEDOT:PSS surfaces. (c) and (d) are the higher magnification images of (a) and (b), respectively.

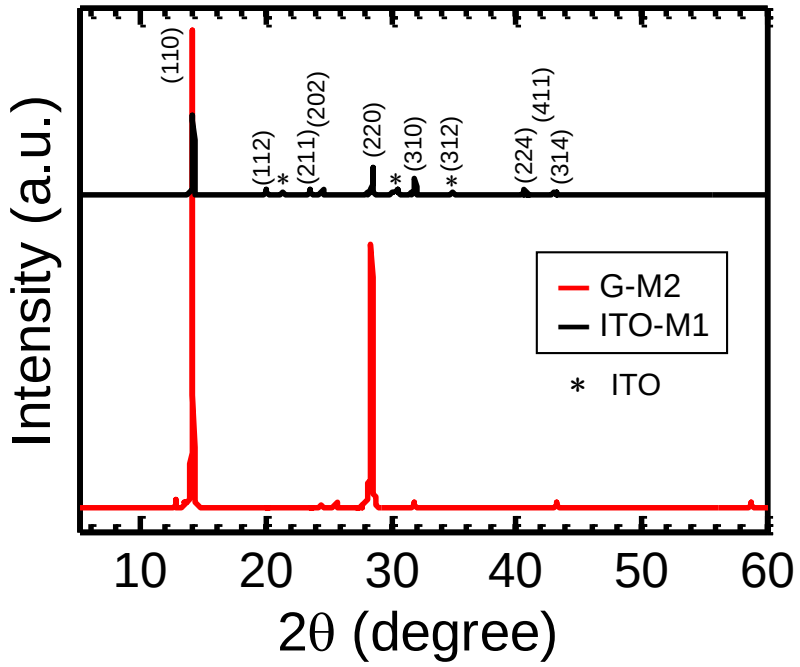

Figure S8. X-ray diffraction patterns of G-M2/PEDOT:PSS/$MAPbI_3$ and ITO-M1/PEDOT:PSS/$MAPbI_3$. Peaks for perovskite films were observed identically in the X-ray diffraction patterns for both G-M2 and ITO-M1 samples although all the peaks were not seen clearly for the G-M2 sample due to the large difference in intensity among them. It is noticeable that the (110) and (220) peak intensities of the G-M2 sample is much stronger than those of the ITO-M1 sample, which implies that the $MAPbI_3$ film was formed with better alignment of the grain orientation on the smoother graphene surface than on the relatively rough ITO surface.